Development and Validation of a Momentum Integral Numerical Analysis Code for Liquid Metal Fast Reactor

Xiangyi Chen[a], Kune Y. Suh[a*]
[a]*Seoul National University, 1 Gwanak-ro, Gwanak-gu, Seoul 151-742, Korea*
[*]*Corresponding author: kysuh@snu.ac.kr*

1. Introduction

Lead-cooled Fast Reactors (LFR) using Pb or Pb-Bi-alloy as the coolant are categorized into Generation IV Nuclear Systems. The coolant thermal-hydraulic characteristics such as very high boiling temperature, good heat transfer ability enable it to have a compact configuration of the reactor core. These features sufficiently cater the requirements to develop small modular reactor with well-known preferences from public concern and investment interest. The initiative of Lead-bismuth eutectic cooled reactor design began from the 1950s in USSR and US, but unlike it is desired today for commercial use, the designs are mainly for the military purpose. The expediency gap between military use and commercial use exists in the capability and neutron spectrum which is a natural barrier of technology migration.

Efforts to fill up the gap have been seen in last several decades. Recently, in the Generation IV International Forum (GIF) framework, advanced modelling and simulation are hit under the spotlight. In Seoul National University, the test loop named HELIOS (Heavy Eutectic Loop Integrated Operation System) was constructed in 2005. Benchmark problems in isothermal steady state forced convection and in natural circulation were taken as the exercise for nine organizations. The result shows considerable uncertainties of handbook correlation predictions of pressure loss in the reactor core [1]. In this work, this benchmark problem is conducted to assess the precision of the upgraded in-house code MINA. Comparison of the results from different best estimate codes employed by various grid spacer pressure drop correlations is carried out to suggest the best one.

2. Experimental Facility

HELIOS is scaled down from the PEACER (Proliferation-resistant Environment-friendly Accident-tolerant Continuable-energy Economical Reactor) - 300 using the general scaling laws for natural-circulation proposed by Ishii and Kataoka [2]. In this scaling process, the elevation difference between hot and cold center keeps the same as about 12 m, but the diameters of piping are reduced. As a result, the fundamental requirement for similarity of the Ri number, Friction number as well as the geometrical similarity are well secured. Table 1 shows the comparison of design parameters between HELIOS and PEACER-300 [1]. The main components of HELIOS consist a core, an expansion tank, a heat exchanger, a mechanical pump, an orifice, five gate valves, nine tee junctions with 9 straight flow direction and one branch flow direction, nine 45º elbows, four 90º elbows and around 14.9 meters long straight pips. Figure 1 shows the 3-D drawing of HELIOS [1]. The heat exchanger and expansion tank are installed at the top of HELIOS while he mockup core and mechanical pump are located at the bottom of the loop. Ten K-type thermocouples are used along the loop to measure the fluid and external wall temperature with accuracy of $\pm$ 0.5 K. Five differential pressure transducers are placed between heat exchanger, expansion tank, gate valve, mockup core and a straight pipe.

3. Numerical Study

In this section an in-house code is described, the detailed hydraulic resistance correlations employed in this calculation are given which include pipe entrance or exit, sudden expansion or contraction, orifices, valves, elbow, discharge into vessel, entrance from vessel to tube, spacers, tees. Most of the correlations used in this calculation are suggested by the report of Phase I isothermal forced convection case in HELIOS published in 2012 except for the correlation used in reactor core which shows considerable deviation from experimental data [1].

3.1 MINA Code

The in-house code Momentum Integral Numerical Analysis (MINA) is employed in this calculation. MINA was originally developed for optimizing liquid metal cooled battery-type reactor in previous work. In this code, constant mass flow rate is assumed in the simulated region; the fluid is considered to be incompressible but thermally expandable. This assumption enables decoupling of the momentum and energy equations in the single-phase flow condition. Thus, the governing equation can be approximated as below [2].
Momentum equation:

$$\int_0^L \frac{\partial G}{\partial t} dz + \left(\frac{G^2}{\rho}\right)_{z=L} - \left(\frac{G^2}{\rho}\right)_{z=0} = P_{z=0} - P_{z=L} - \int_0^L \frac{f|G|G}{2D_e\rho} dz - \int_0^L \rho g dz \quad (1)$$

where G is mass flux, ρ is density of Pb-Bi, P is pressure, L is the axial length.

For loop geometry, Eq. (1) is integrated over the loop:

$$\oint \frac{\partial G}{\partial t} dz = -\oint \frac{f|G|G}{2D_e\rho} dz - \oint \rho g dz \qquad (2)$$

Rewriting (2) using mass flow rate ($\dot{m}$) gives:

$$\frac{\partial \dot{m}}{\partial t} \oint \frac{1}{A} dz = -\oint \frac{f|\dot{m}|\dot{m}}{2D_e\rho A^2} dz - g \oint \rho dz \qquad (3)$$

After including form loss term (K) to the above equation, it is discretized as:

$$\frac{\dot{m}^{n+1} - \dot{m}^n}{\Delta t} \left(\sum_i \frac{\Delta z_i}{A_i} \right) = -\left(\sum_i \frac{f_i \Delta z_i}{2\rho_i D_{ei} A_i^2} + \sum_j \frac{K_j}{2\rho_i A_j^2} \right) |\dot{m}^{n+1}| \dot{m}^{n+1} + g \sum_i \rho_i \Delta z_i cos\theta_i \qquad (4)$$

Through this upgrading work, the code structure is optimized, the user interface (U/I) are improved, and the model library is established independently. Previously, MINA was developed by process-oriented programming structure. As a consequence, this type of programming renders it inconvenient to handle the step-dependent geometry variation and detailed adopted simulation in an optimization work. By coupling Python and C++ programming language, the object-oriented programming paradigm was used in this development. The restructured MINA has emphasized its perfect readability, modifiability and maintainability. The database for models of components frequently countered in nuclear systems are expanded, and their flow resistance are based on well-known correlations in both classic handbook and up-to-date correlations newly published. Components are connected by a module called Connector which transfer the incoming properties from previous component and also transfer the exit fluid properties to the next component. And all the components governing equations with their boundary conditions are solved in a module named MINA-solver.

3.2 Friction Factor

The Darcy-Weisbach friction factor models utilized in this application are from Moody Chart. It is divided into three regimes: laminar; laminar-turbulent transition; and turbulent flow regimes. For laminar flow, Hagen-Poiseuille Correlation is used. In turbulent regime, MINA use the Zigrang-Sylvester approximation to Coolebrook-White correlation. The friction factor in transition regime is calculated by interpolation of friction factor at Reynolds number at 3000 and 2200:

Table I: Comparison of design parameters for PEACER-300 and for HELIOS

Parameter	PEACER-300	HELIOS	Ratio of PEACER-300 to HELIOS
Number of loops	3	1	-
Decay heat [MWt] (10% of normal power)	85	0.0174	4 885
Number of rods	77280	4	19 320
LBE flow area [m^2]	6.92	0.00142	4 873
Cross sectional heated area [m^2]	4.2	0.000507	8 284
Natural circulation flow rate [kg/s]	12550	2.4	5 229
ΔT (between hot leg and cold leg) [^oC]	46.8	49.4	0.95
Representative flow velocity at core [m/s]	0.176	0.173	1.02
Elevation difference between thermal centers [m]	8	7.6	1.05
Total loss coefficient	30.4	24.5	1.24
Richardson number	15.2	12.2	1.25

$$f = \frac{64}{\mathrm{Re}} \quad \text{for} \quad 0 < \mathrm{Re} \leq 2200, \tag{5}$$

$$f = \left(3.75 - \frac{8250}{\mathrm{Re}}\right)(f_{\mathrm{Re}=3000} - f_{\mathrm{Re}=2200}) + f_{\mathrm{Re}=2200}$$

$$\text{for} \quad 2200 < \mathrm{Re} < 3000, \tag{6}$$

$$\frac{1}{\sqrt{f}} = -2\lg\left\{\frac{\varepsilon}{3.7\mathrm{D_h}} + \frac{2.51}{\mathrm{Re}}[1.14 - 2\lg(\frac{\varepsilon}{\mathrm{D_h}} - \frac{21.25}{\mathrm{Re}^{0.9}})]\right\}$$

$$\text{for} \quad \mathrm{Re} \geq 3000. \tag{7}$$

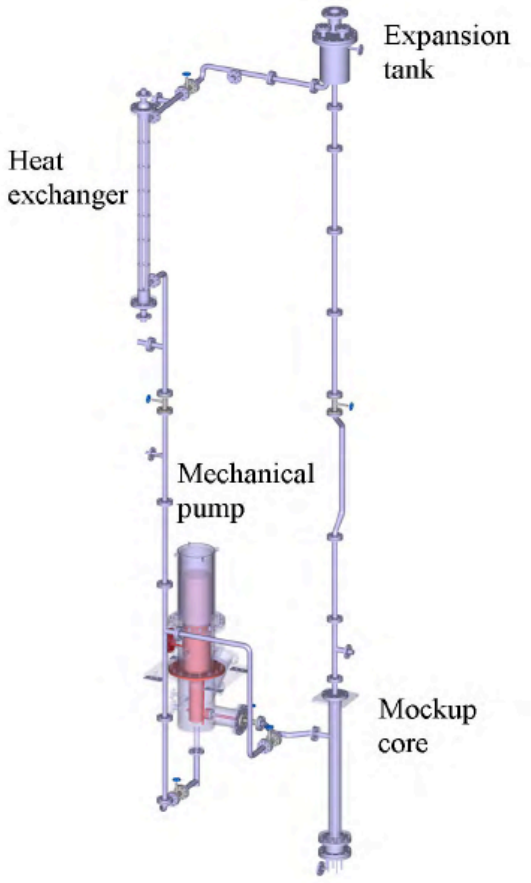

Fig. 1. Three-dimensional diagram of the HELIOS forced convection test setup

3.3 Form loss coefficients

The available form loss coefficients for HELIOS application are pipe entrance or exit, sudden expansion or contraction, orifices, valves, elbow, spacers, tees.

For a sudden expansion, the equation below is applied:

$$K = \left(1 - \frac{A_1}{A_0}\right)^2 \tag{8}$$

For a sudden contraction, the empirical loss coefficient is:

$$K = 0.5 - 0.7\left(\frac{A_0}{A_1}\right) + 0.2\left(\frac{A_0}{A_1}\right)^2 \tag{9}$$

where A_1 is upstream area and A_0 is downstream area.

For fully opened gate valve with geometry in Figure 2 is treated as a combination of contraction and expansion.

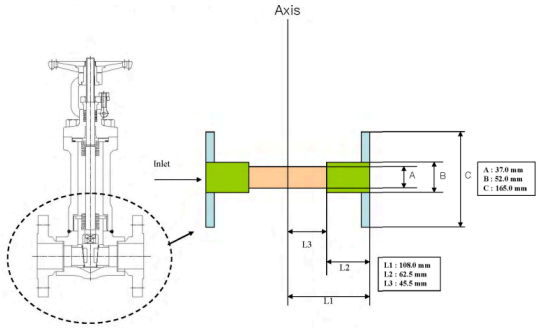

Fig. 2. Gate Valve (Flow Area Section View) in HELIOS

For a elbow shown in Figure 3, the form loss coefficient is calculated by:

$$K = K_{\mathrm{Re}} \cdot K_{loc} + K_{\mathrm{fr}} \tag{10}$$

$$K_{\mathrm{fr}} = 0.0175 \cdot \frac{R_o}{D_o} \cdot \Phi \cdot \lambda \tag{11}$$

$$K_{\mathrm{loc}} = A_1 \cdot B_1 \tag{12}$$

where A_1 and B_1 are taken from Table II and Table III; K_{Re} is shown in Table IV.

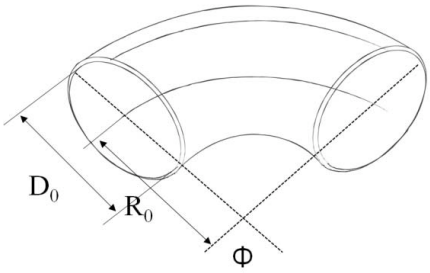

Fig. 3. Geometry of the Elbow

Table II: Values of A_1 for elbow form factor

δ	20.0	30.0	45.0	60.0	75.0
A_1	0.31	0.45	0.60	0.78	0.90
δ	90.0	110.0	130.0	150.0	180.0
A_1	1.00	1.13	1.20	1.28	1.40

Table III: Values of B_1 for elbow form factor

R_0/D_0	0.50	0.60	0.70	0.80	0.90
B_1	1.18	0.77	0.51	0.37	0.28
R_0/D_0	1.00	1.25	0.50	2.00	4.00
B_1	0.21	0.19	0.17	0.15	0.11

Table IV: Values of K_{Re} for elbow form factor

Values of K_{Re}						
R_0/D_0	$\mathrm{Re}\times10^{-5}$					
	0.10	0.14	0.20	0.30	0.40	0.60
0.5-0.55	1.40	1.33	1.26	1.19	1.14	1.09
>0.55-0.70	1.67	1.58	1.49	1.40	1.34	1.26
>0.70	2.00	1.89	1.77	1.64	1.56	1.46
R_0/D_0	$\mathrm{Re}\times10^{-5}$					
	0.80	1.00	1.40	2.00	3.00	4.00
0.5-0.55	1.06	1.04	1.00	1.00	1.00	1.00
>0.55-0.70	1.21	1.19	1.17	1.14	1.06	1.00
>0.70	1.38	1.30	1.15	1.02	1.00	1.00

For an orifice, the value of form loss coefficient is given by:

$$K = \left(\frac{F_1}{F_0}\right)^2 \left(1 + 0.707\sqrt{1 - \frac{F_0}{F_1}} - \frac{F_0}{F_1}\right)^2 \qquad (13)$$

For a tee-elbow, table V gives the form loss coefficient, it depends on the ratio of inlet flow rate *Wa* and the outlet flow rate *Wz*. In this simulation, tee-straight is considered to be straight pipe.

Table V: Values of *K* for Tee-elbow form factor

Wa/Wz	0	0.2	0.4
K	0.98	0.87	0.9
Wa/Wz	0.6	0.8	1
K	0.98	1.12	1.29

For entrance in tubes and discharge into a vessel shown in Figure 3 and Figure 4, the form loss coefficients are given in Table VI and Table VII respectively.

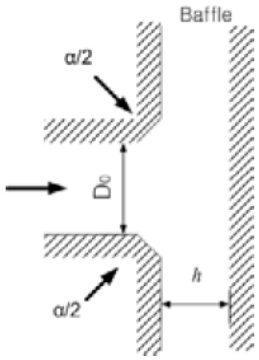

Fig. 3. Discharge into a vessel

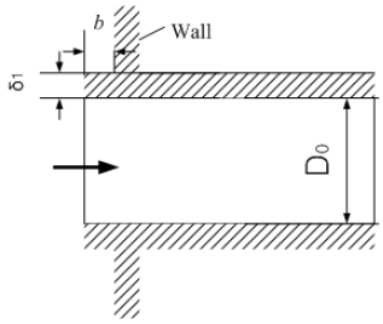

Fig. 4. Entrance in tubes

Table VI: Values of *K* for Entrance in Tubes from Vessel

$\frac{\delta_1}{D_h}$	b/D_h										
	0	0.002	0.005	0.010	0.020	0.050	0.10	0.20	0.30	0.50	∞
0	0.50	0.57	0.63	0.68	0.73	0.80	0.86	0.92	0.97	1.00	1.00
0.004	0.50	0.54	0.58	0.63	0.67	0.74	0.8	0.86	0.9	0.94	0.94
0.008	0.50	0.53	0.55	0.58	0.62	0.68	0.74	0.81	0.85	0.88	0.88
0.012	0.50	0.52	0.53	0.55	0.58	0.63	0.68	0.75	0.79	0.83	0.83
0.016	0.50	0.51	0.51	0.51	0.55	0.58	0.64	0.7	0.74	0.77	0.77
0.020	0.50	0.51	0.51	0.51	0.52	0.55	0.60	0.66	0.69	0.72	0.72
0.024	0.50	0.50	0.50	0.50	0.51	0.53	0.58	0.62	0.65	0.68	0.68
0.030	0.50	0.50	0.50	0.50	0.52	0.52	0.54	0.57	0.59	0.61	0.61
0.040	0.50	0.50	0.50	0.50	0.51	0.51	0.51	0.52	0.52	0.54	0.54
0.050	0.50	0.50	0.50	0.50	0.50	0.50	0.50	0.50	0.50	0.50	0.50
∞	0.50	0.50	0.50	0.50	0.50	0.50	0.50	0.50	0.50	0.50	0.50

Table VII: Values of *K* for Discharge into a Vessel

h/D_0										
α. deg	0.1	0.15	0.2	0.25	0.3	0.4	0.5	0.6	0.7	1.0
0	-	-	-	-	-	-	1.37	1.02	1.11	1.00
15	-	-	-	1.50	1.06	0.72	0.61	0.59	0.58	0.58
30	-	-	1.23	0.79	0.66	0.64	0.66	0.66	0.67	0.67
45	-	1.50	0.85	0.73	0.75	0.79	0.81	0.82	0.82	0.82
60	-	0.98	0.76	0.80	0.90	0.96	1.00	1.01	1.02	1.02
90	1.50	0.72	0.74	0.83	0.89	0.94	0.96	0.98	1.00	1.00

For grid spacers shown in figure 5, the In's method is modified and used in this calculation shown in Equation (14) [3][4]. Equation (17) shown is modified from the original formulation (16) for the reason of low mass flow rate when comparing to PWR. The effect of the modification is presented in figure 6.

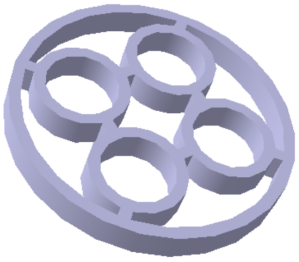

Fig. 5. Grid spacer in HELIOS

The formulation for the loss coefficient K_{grid} is

$$K_{grid} = C_{grid}^{form}\frac{\epsilon}{(1-\epsilon)^2} + C_{grid}^{fric}\frac{A_{grid,wetted}}{A_{flow,bundle}}\frac{1}{(1-\epsilon)^2}$$

$$+C_{rod}^{fric}\frac{A_{rods,wetted@grid}}{A_{flow,bundle}}\frac{1}{(1-\epsilon)^2} \quad (14)$$

where:

In the first term on the right:

$$C_{grid}^{form} = 2.75 - 0.27\log_{10}Re_{away\ from\ grid} \quad (15)$$

In the second term on the right:

Original formulation is

$$C_{d,grid}^{fric} = C_{d,lam}^{fric}\frac{L_t}{H} + C_{d,tur}^{fric}\frac{H-L_t}{H}$$

$$\text{for } H \geq 3\times10^4\frac{\mu_{avg}}{G_{@grid}H} \quad (16a)$$

$$= 3\times10^4\frac{\mu_{avg}}{G_{@grid}H}$$

$$\text{for } H < 3\times10^4\frac{\mu_{avg}}{G_{@grid}H} \quad (16b)$$

The modified formulation is

$$C_{d,grid}^{fric} = C_{d,lam,@L_t}^{fric} + C_{d,tur,@H}^{fric} - C_{d,tur,@L_t}^{fric}$$

$$\text{for } H \geq 3\times10^4\frac{\mu_{avg}}{G_{@grid}H} \quad (17a)$$

$$= 3\times10^4\frac{\mu_{avg}}{G_{@grid}H}$$

$$\text{for } H < 3\times10^4\frac{\mu_{avg}}{G_{@grid}H} \quad (17b)$$

In the third term on the right:

$$C_{rod}^{fric} = 0.184Re_{@grid}^{-0.2} \quad (18)$$

ϵ: ratio between the total projected grid cross section and the bundle flow area away from the grid;
$C_{d,tur,@L_t}^{fric}$: integrated drag coefficient during turbulence region with characteristic length.
$C_{d,grid}^{fric}$: integrated drag coefficient during spacer thickness;
$C_{d,lam,@L_t}^{fric}$: integrated drag coefficient during laminar region with characteristic length L_t;
$C_{d,tur,@H}^{fric}$: integrated drag coefficient during turbulence region with characteristic length H (grid spacer thickness).

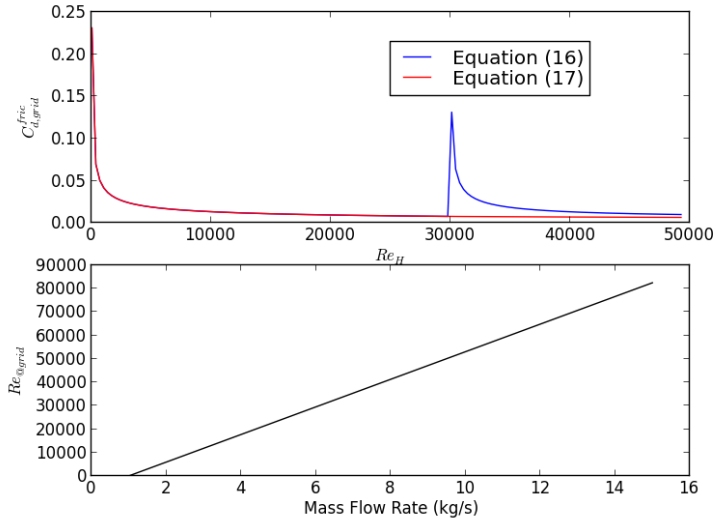

Fig. 6. Comparison between Eq. (16) and Eq. (17)

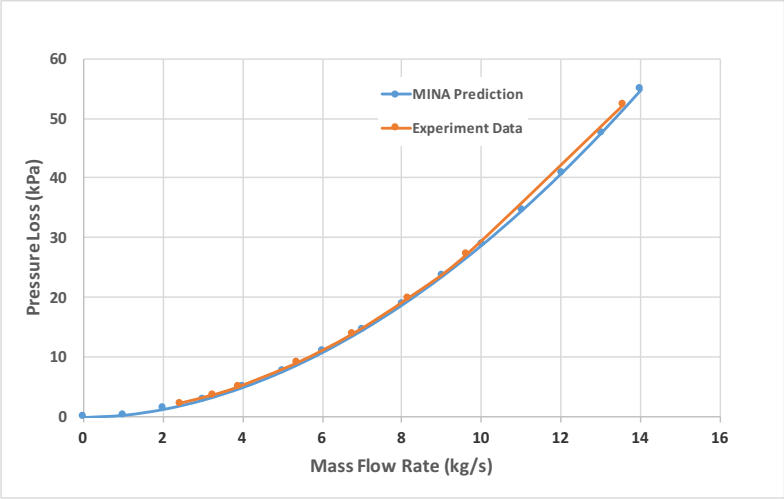

Fig. 7. Comparison between MINA prediction and Measured Pressure loss in HELIOS core region

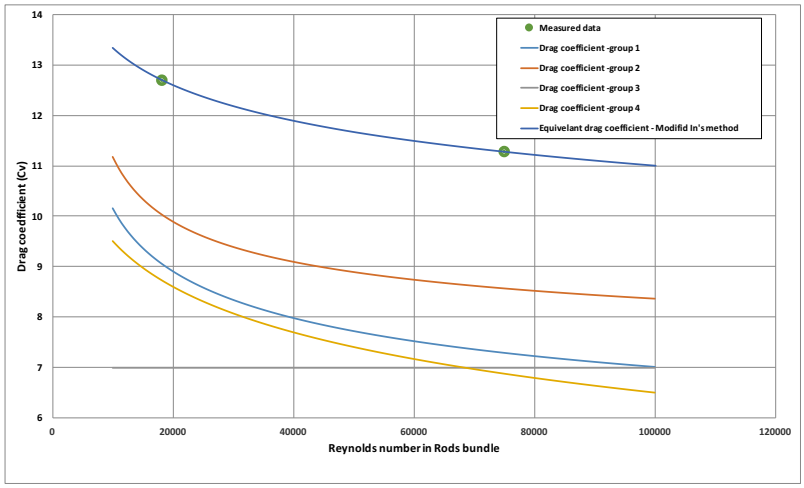

Fig. 8. Drag coefficient comparison between Rehme's method and In's method

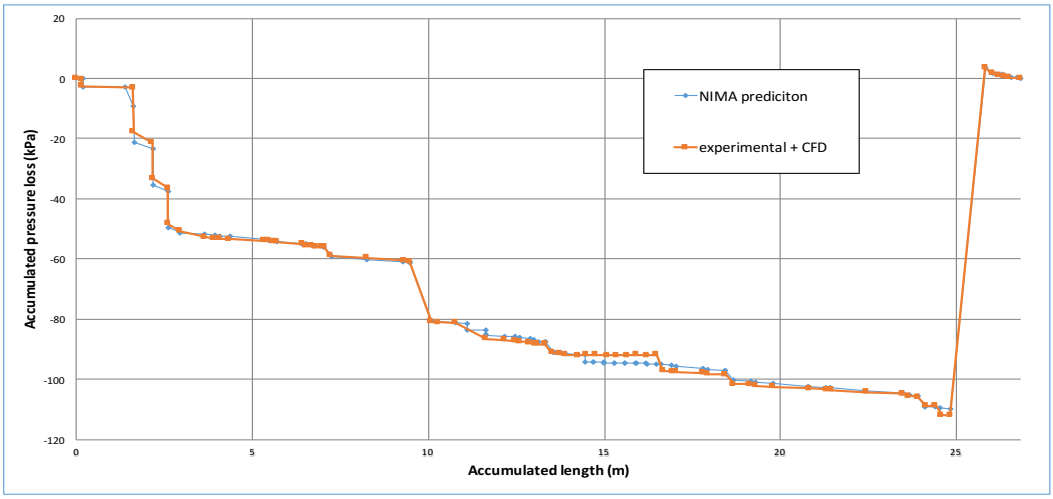

Fig. 9. Comparison of the accumulated pressure loss at 13.5 kg/s mass flow rate case

4. Result and Conclusion

As mentioned in the previous section, the predictions of pressure loss in the reactor core in earlier works by nine organizations shows significant deviations from the experiment which need the search for a more reasonable correlation. By modifying In's method, it presents good agreement with the experiment data which is shown in Figure 7. The reason for the failure of the prediction in previous work is caused by the utilization of Rehme's method which is categorized into four groups according to different fitting strategy [1]. Through comparison of drag coefficients calculated by four groups of Rheme's method, equivalent drag coefficient calculated by In's method and experiment data shown in Figure 8, we can conclude that Rehme's method considerably underestimate the drag coefficients in grid spacers used in HELIOS and In's method give a reasonable prediction. Starting from the core inlet, the accumulated pressure losses are presented in figure 9 along the accumulated length of the forced convection flow path; the good agreement of the prediction from MINA with the experiment result shows MINA has very good capability in integrated momentum analysis makes it robust in the future design scoping method development of LFR.

REFERENCES

[1] Cho, Jae Hyun, et al. "Benchmarking of thermal hydraulic loop models for Lead-Alloy Cooled Advanced Nuclear Energy System (LACANES), phase-I: Isothermal steady state forced convection." *Journal of Nuclear Materials*415.3 (2011): 404-414.
[2] Lee, Il S., and Kune Y. Suh. "Full-height thermal-hydraulic scaling analysis of Pb-Bi-cooled fast reactor peacer." *Nuclear technology* 155.3 (2006): 265-281.
[3] In, Wang Kee, Dong Seok Oh, and Tae Hyun Chun. "Empirical and computational pressure drop correlations for pressurized water reactor fuel spacer grids." *Nuclear technology* 139.1 (2002): 72-79.
[4] Todreas, Neil E., and Mujid S. Kazimi. *Nuclear systems: thermal hydraulic fundamentals*. Vol. 1. CRC Press, 2012.